Pergamon

Acta Materialia 50 (2002) 3579–3595

www.actamat-journals.com

A reaction-layer mechanism for the delayed failure of micron-scale polycrystalline silicon structural films subjected to high-cycle fatigue loading

C.L. Muhlstein [a], E.A. Stach [b], R.O. Ritchie [a,*]

[a] *Materials Sciences Division, Lawrence Berkeley National Laboratory, and Department of Materials Science and Engineering, University of California, Berkeley, CA 94720-1760, USA*

[b] *National Center for Electron Microscopy, Lawrence Berkeley National Laboratory, Berkeley, CA 94720-1760, USA*

Received 5 November 2001; received in revised form 18 March 2002; accepted 18 March 2002

Abstract

A study has been made to discern the mechanisms for the delayed failure of 2-μm thick structural films of n^+-type, polycrystalline silicon under high-cycle fatigue loading conditions. Such polycrystalline silicon films are used in small-scale structural applications including microelectromechanical systems (MEMS) and are known to display 'metal-like' stress-life (*S/N*) fatigue behavior in room temperature air environments. Previously, fatigue lives in excess of 10^{11} cycles have been observed at high frequency (~40 kHz), fully-reversed stress amplitudes as low as half the fracture strength using a surface micromachined, resonant-loaded, fatigue characterization structure. In this work the accumulation of fatigue-induced oxidation and cracking of the native SiO_2 of the polycrystalline silicon was established using transmission electron and infrared microscopy and correlated with experimentally observed changes in specimen compliance using numerical models. These results were used to establish that the mechanism of the apparent fatigue failure of thin-film silicon involves sequential oxidation and environmentally-assisted crack growth solely within the native SiO_2 layer. This 'reaction-layer fatigue' mechanism is only significant in thin films where the critical crack size for catastrophic failure can be reached by a crack growing within the oxide layer. It is shown that the susceptibility of thin-film silicon to such failures can be suppressed by the use of alkene-based monolayer coatings that prevent the formation of the native oxide. © 2002 Acta Materialia Inc. Published by Elsevier Science Ltd. All rights reserved.

Keywords: Silicon; Fatigue; Thin films; MEMS; Self-assembled monolayer coatings

1. Introduction

The promise of revolutionary commercial products at small dimensions has fueled the rapid development of microelectromechanical systems (MEMS) and the enabling technologies of surface micromachining. Silicon-based structural films have emerged as the dominant material system for MEMS because the micromachining technologies for silicon are readily adapted from the microelectronics industry, and are compatible with fabrication strategies for the integrated circuits necessary for actuation and control of the systems.

* Corresponding author: Tel.: +1-510-486-5798; fax: +1-510-486-4881.

E-mail addresses: cmuhlstn@uclink4.berkeley.edu (C.L. Muhlstein); roritchie@lbl.gov (R.O. Ritchie).

1359-6454/02/$22.00 © 2002 Acta Materialia Inc. Published by Elsevier Science Ltd. All rights reserved.
PII: S1359-6454(02)00158-1

However, the long-term durability of these microsystems may be compromised by the susceptibility of thin-film silicon to delayed failure during cyclic loading conditions in ambient air [1–8].

Cyclic fatigue is the most commonly encountered mode of failure in structural materials, occurring in both ductile (metallic) and brittle (ceramic) solids (although the mechanisms are quite different) [9]. The mechanistic understanding of fatigue together with the use of damage/fracture mechanics to describe its effect at continuum dimensions has allowed for the reliable design and operation of innumerable macro-scale structures, such as aircraft airframes and engines. At the micro-scale, the fatigue of ductile materials is attributed to cyclic plasticity involving dislocation motion that causes alternating blunting and resharpening of a pre-existing crack tip as it advances [10]. In contrast, brittle materials invariably lack dislocation mobility at ambient temperatures, such that fatigue occurs by cycle-dependent degradation of the (extrinsic) toughness of the material in the wake of the crack tip that developed from preexisting material inhomogeneities [11]. Prior to this work, the relevance of these fatigue mechanisms to silicon films had yet to be established.

Silicon is generally regarded as a prototypical brittle material; dislocation activity is generally not observed at low homologous temperatures (below ~500 °C) and there is little evidence of extrinsic toughening, such as grain bridging or microcracking [12]. Moreover, silicon is not susceptible to environmentally-induced cracking (i.e., stress-corrosion cracking) in moist air or water [13–15] at growth rates measurable in bulk specimens. *These observations strongly suggest that silicon should not fatigue at room temperature.* Indeed, there has been no evidence to date that bulk silicon is susceptible to fatigue failure. However, there is substantial evidence that cyclically-stressed, micron-scale, silicon films can fail prematurely under high-cycle fatigue loading [1–8,16].

The observation that silicon thin films can fail under cyclic loading was first reported by Connally and Brown a decade ago [1]. Since then, the present authors and others [2–7] have confirmed that 2 to 20 μm thick single crystal and polycrystalline silicon films can fail in fatigue at stresses as low as half their (single-cycle) fracture strength after more than ~10^{11} cycles. Despite such results, the mechanistic origins of why thin-film silicon should apparently suffer fatigue failure have remained elusive. Early studies highlighted the importance of water vapor and speculated that the mechanism may be associated with static fatigue of the native silica layer [1,7]. Other proposed explanations have involved dislocation activity in compression-loaded silicon (e.g., [17]), stress-induced phase transformations [4], and impurity effects [4], although in no instance has conclusive experimental evidence been presented to support any of these mechanisms. Moreover, until now there has never been any direct observation of fatigue damage in micron-scale silicon, nor indications on how it accumulates.

A recent study by the authors [18], however, provided the initial experimental evidence that the crack initiation and growth processes involved in the apparent fatigue of silicon are confined to the amorphous SiO_2 reaction layer that forms on surfaces upon their exposure to air. In this paper, we present a mechanism for the apparent fatigue of silicon, termed reaction-layer fatigue, on the basis of prior stress-life fatigue data, a compliance technique for monitoring the damage accumulation, and microstructural analysis using high-voltage transmission electron microscopy. Additionally, we suggest a method for suppressing the cyclic fatigue of silicon films through the use of alkene-based monolayer coatings that is validated with stress-life fatigue data.

2. Experimental procedures

The 2-μm thick silicon films were fabricated from the first structural polycrystalline silicon layer on run 18 of the MCNC/Cronos MUMPs™ process. This surface micromachining process utilizes low-pressure chemical vapor deposition (LPCVD) to manufacture n^+-type (resistivity, ρ=1.9 × 10^{-3} Ω·cm) polycrystalline silicon [19]. Wafer curvature measurements showed the film to have a compressive residual stress of about 9 MPa [19]; out-of-plane deformation due to a through-thickness

residual stress gradient could not be detected using white-light interferometry. Secondary ion mass spectroscopy (SIMS), referenced to known standards, was used to quantify the concentration of hydrogen, carbon, oxygen, and phosphorous present.

The elastic properties of polycrystalline silicon thin films approach the average behavior of idealized polycrystalline materials. An average of the Voigt and Reuss bounds for a random, polycrystalline aggregate (Young's modulus, E=163 GPa, Poisson's ratio, ν=0.23 [20]) were used to estimate the elastic behavior of the material. The fracture strength of polycrystalline silicon typically ranges from 3 to 5 GPa depending on loading condition, specimen size, and test technique. The fracture toughness, K_c, is ~1 MPa$\sqrt{\text{m}}$ [12,21].

The microstructure of the films was characterized using transmission electron microscopy (TEM). Cross-sectional TEM specimens were prepared from the patterned films using standard laboratory practices [22]. Pairs of patterned chips containing the surface micromachined structures were glued together face-to-face, mechanically thinned, dimpled, and ion milled to the desired electron transparency. Diffraction contrast and high-resolution microscopy of the these specimens was performed using the Berkeley JEOL Atomic Resolution Microscope (ARM) at an operating voltage of 800 kV and a JEOL 3010 TEM operating at 300 kV. Analytical characterization was accomplished using a Philips CM200 Field Emission microscope equipped with a Link Energy Dispersive Spectrometer (EDS) and a Gatan Image Filter for electron energy loss spectroscopy (EELS) and energy filtered imaging (EFTEM). Plan view observations of the grain morphology and oxide structure were accomplished using both the ARM and the Kratos High Voltage Electron Microscope (HVTEM) operating at 0.8–1.0 MeV. Plan view samples were prepared by simply lifting the micromachined structures off of the substrate using a tungsten probe tip and placing them onto 100 mesh clam shell grids. For HVTEM studies, no additional thinning was necessary to image through the entire 2 μm thick samples.

The stress-life (*S/N*) fatigue behavior of the polycrystalline silicon films was determined using a ~300-μm square, ~2-μm thick, surface micromachined fatigue characterization structure, as described in ref. [5] (Fig. 1). Briefly, the notched cantilever beam specimen (~40-μm long, 19.5-μm wide, with a 13-μm deep, ~1 μm root radius notch) is attached to a large, perforated, plate-shaped mass and is electrostatically forced to resonate. On opposite sides of the resonant mass are interdigitated 'fingers' commonly known as 'comb drives'; one side is for electrostatic actuation, the other provides capacitive sensing of motion. The specimen is attached to an electrical ground, and a sinusoidal voltage (with no direct-current (DC) offset) at half the natural frequency is applied to one comb drive, thereby inducing a resonant response in the plane of the figure. These conditions generate fully reversed, constant amplitude, sinusoidal stresses at the notch, i.e., a load ratio (ratio of minimum to maximum load) of $R=-1$, that are controlled to better than 1% precision with a resolution of ~5%. Specimens were cycled to failure at resonance (~40 kHz) in ambient air (~25 °C, 30–50% relative humidity) at stress amplitudes ranging from ~2 to 4 GPa using the control scheme described in refs. [4,5].

Specimens were prepared by removing the sacrificial oxide layer in 49% aqueous hydrofluoric acid (HF) for $2^1/_2$ or 3 min, drying at 110 °C in air, and subsequently mounting in ceramic electronic packages for testing [5]. In an attempt to suppress formation of the native oxide and access of moisture to the silicon surface, specific specimens were coated with an alkene-based monolayer of 1-octadecene, $C_{16}H_{33}CH{=}CH_2$, after removal of the sacrificial oxide. The monolayer was then applied to the surface of the silicon in a reactor containing a solution of one part 1-octadecene in nine parts hexadecane [23]. This hydrophobic monolayer bonds directly to the hydrogen-terminated surface atoms of the silicon film created by the exposure to hydrofluoric acid such that no oxide can form; it acts as an effective barrier to both oxygen and water [23].

The experimentally-measured motion of the resonating fatigue characterization structure was used to determine the applied stress amplitude, natural frequency, and to monitor the accumulation of fatigue damage prior to failure. The magnitude

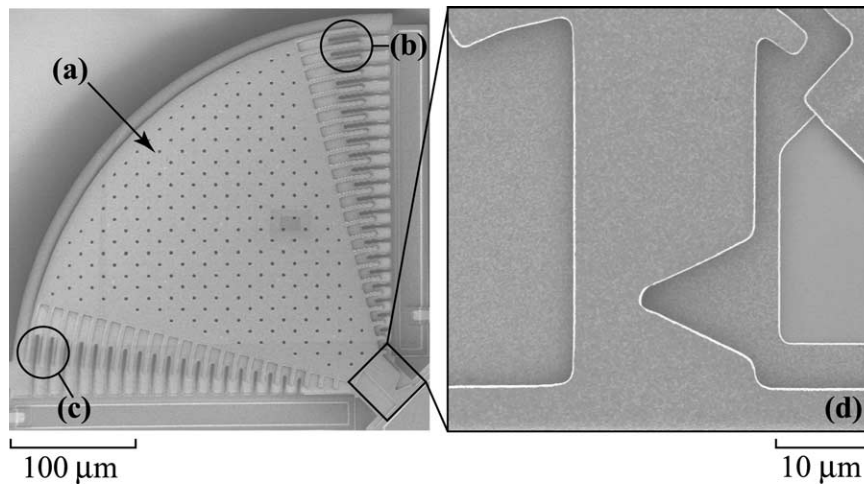

Fig. 1. Scanning electron micrograph of the fatigue life characterization structure and notched cantilever beam specimen used in this investigation. The (a) mass, (b) comb drive actuator, (c) capacitive displacement sensor, and (d) notched cantilever beam specimen (inset) are shown.

of the displacements was carefully calibrated, as detailed in ref. [5]. Finite element models were used to establish the relationship between the displacements and the maximum principal stress at the notch. It was previously demonstrated that measured changes in natural frequency may be attributed to damage accumulation in the specimen [7,24]. Thus, additional numerical models of structures containing cracks were used to determine the relationship between crack length and natural frequency (i.e., compliance) and the stress-intensity factor, K. The models were constructed using a commercial software package (ANSYS v. 5.7); full details are reported in ref. [25]. In the present paper, such methods were used to measure in situ the propagation of nanometer-scale cracks by monitoring the change in natural frequency of the sample. Crack-growth rates were determined using a modified secant method applied over ranges of crack extension of 2 nm with a 50% overlap with the previous calculation window; the average crack-growth rate was calculated based on a linear fit of the experimental data. The maximum stress intensity immediately prior to failure was taken as an estimate of the fracture toughness of the material.

After testing, the crack path and fracture surfaces of the specimens were characterized using scanning electron microscopy (SEM) and HVTEM. To avoid corrupting any microstructural or fractographic features, neither SEM conductive coatings nor TEM thinning processes were used.

To evaluate the possibility of specimen heating due to the large amplitude, high frequency stresses and the induced electrical current used to measure motion of the structure, high-resolution infrared (IR) imaging of the fatigue characterization structure was performed in order to map temperature changes during testing. Thermal images were generated by plotting the difference between IR images (12-bit resolution) collected while the structure was resonated at a constant stress amplitude, and at rest. Individual IR images were collected by averaging over 2 sec at an acquisition rate of 50 Hz. Temperature changes as small as 20 mK could be detected with a spatial resolution of better than 8 μm.

3. Results

3.1. Microstructural analysis

The microstructural analysis of the 2-μm thick polycrystalline silicon film, shown in the cross-sectional TEM image of Fig. 2a, revealed an equiaxed

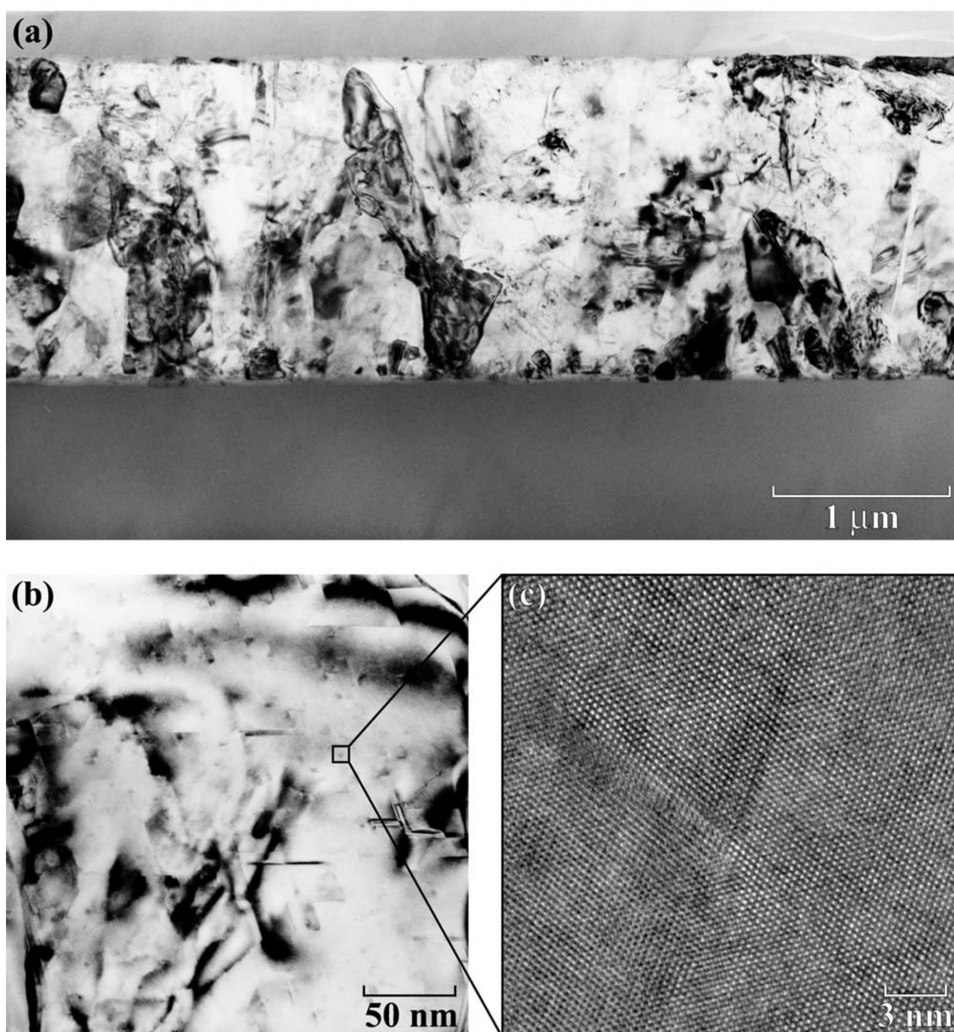

Fig. 2. (a) Microstructure of the polycrystalline silicon structural film showing a typical cross-sectional TEM image of the through-thickness grain morphology. TEM images of defect types, showing: (b) 220 bright field image of the interior of the grain to highlight microtwins, stacking faults, and Lomer–Cottrell dislocation locks, (c) high resolution image of a Lomer–Cottrell lock (inset).

grain morphology (grain size of ~100 nm), with no evidence of strong texture (from corresponding selected-area diffraction). No variations in microstructure were apparent near features such as the root of the notch, as expected given the deposition and etching strategy used in the surface micromachining process. The lack of a textured columnar structure, which is routinely observed in thin-film silicon [26], may be a result of the 900°C annealing used to dope the silicon with phosphorous and relax the residual stresses associated with growth of the film.

SIMS analysis of the contaminants present revealed the interior of the film to contain ~ 2×10^{18} atoms/cm^3 hydrogen, 1×10^{18} atoms/cm^3 oxygen, and 6×10^{17} atoms/cm^3 carbon [5], levels which are consistent with the processing history of the film. In addition, 1×10^{19} atoms/cm^3 of phosphorous were detected from the phosphosilicate glass used to dope the film. The films were found

to be representative of materials used throughout micromachining and MEMS research and production. Oxygen concentrations in excess of $\sim 10^{18\ \mathrm{atoms/cm^3}}$ at room temperature can be associated with precipitation of amorphous and crystalline Si-O phases [27], although EELS of the interior of the grains revealed no segregation of oxygen or carbon in the film. Similarly, EFTEM imaging revealed no segregation of oxygen, carbon, phosphorous, or nitrogen within the detectability limits of the technique. We conclude that that no precipitation of secondary species exists in the films.

Diffraction contrast imaging was used to characterize the defect structure of the film and to confirm the absence of precipitation. A high magnification 220 bright field image of the interior of a representative grain, shown in Fig. 2b, reveals several different types of lattice defects, including Lomer–Cottrell dislocation locks (a high resolution image of which is depicted in Fig. 2c), microtwins, and stacking faults. All dark areas of contrast in these cross sectional images, including polygonal features, were observed to correspond to one of these types of lattice defects and not to the presence of precipitates.

3.2. Stress-life fatigue behavior

Stress-life (*S/N*) data for the polycrystalline silicon films from ref. [5], based on a total of 28 fatigue specimens tested in room air, is shown in Fig. 3; fatigue lives, N_f, varied from ~10 sec to 34 days (3×10^5 to 1.2×10^{11} cycles) for stress amplitudes ranging from ~2 to 4 GPa at $R=-1$. Two specimens were interrupted prior to failure for examination in the HVTEM. It is apparent that the polycrystalline silicon films display 'metal-like' *S/N* behavior, with an endurance strength at 10^9–10^{10} cycles of roughly half the (single-cycle) fracture strength. Similar behavior has been seen in 20-μm thick films of single-crystal silicon cycled under similar conditions [4]. Stress-life fatigue tests were also conducted on specimens coated with the 1-octadecene monolayer. Thirteen specimens were tested to failure and five were interrupted prior to failure for examination in the HVTEM. Fatigue lives varied from ~7.5 sec to 25 days (3×10^5 to 8.9×10^{10} cycles) for stress amplitudes ranging from ~1.4 to 3.3 GPa at $R=-1$ (Fig. 4a). In contrast to the specimens without the monolayer coating, the behavior is reminiscent of bulk brittle materials.

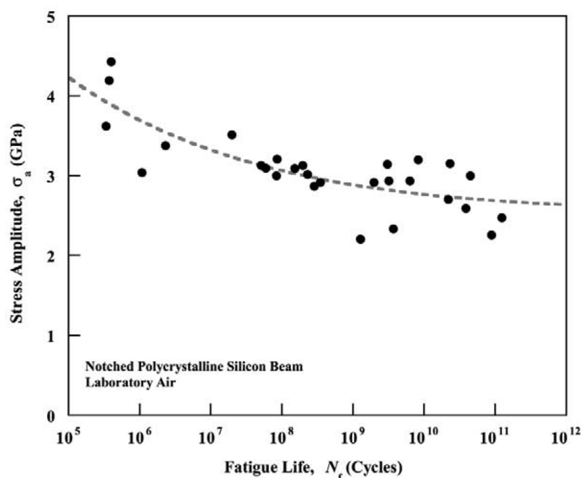

Fig. 3. Typical stress-life (S/N) fatigue behavior of the 2 μm-thick, polycrystalline silicon at ~40 kHz in moist room air under fully reversed, tension–compression loading [5].

3.3. Fractography and crack-path analysis

SEM and TEM of both failed specimens and specimens interrupted during testing were used to evaluate fatigue damage, including the nature of the crack trajectory and the fracture surface morphology. Previous work [5] established that crack paths in polycrystalline silicon films during fatigue and subsequent overload failure are transgranular. Scanning electron microscopy at magnifications as high as 80,000× revealed a cleavage fracture mode with few distinctions in fracture surface morphology in the (presumed) fatigue and overload regimes.

3.3.1. Overload fractures

Overload fracture surfaces were (unambiguously) created by manually loading the fatigue test structure with a fixed (non-cyclic) displacement under an optical microscope; these conditions generate cracks that arrest due to the decreasing stress gradient associated with displace-

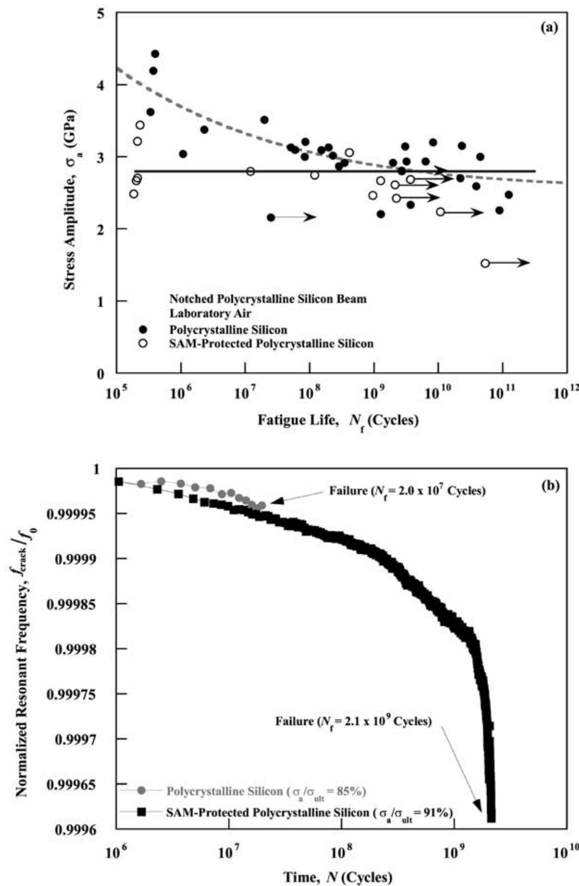

Fig. 4. Comparison of the fatigue behavior of uncoated and monolayer-coated polycrystalline silicon thin films, showing (a) the respective *S/N* curves and (b) accumulated fatigue damage in terms of the change in natural frequency of the sample, f_{crack}, normalized by the natural frequency at the start of the test, f_0. Note the reduced susceptibility of the coated polycrystalline silicon films to fatigue failure in (a), and the significantly enhanced life (by two orders of magnitude) compared to uncoated polycrystalline silicon at comparable applied stress amplitudes in (b).

ment-control in this configuration. Cracking in the silicon was confirmed to be transgranular cleavage (Fig. 5), with evidence of secondary cracking and microcracking consistent with the 'slivers' which appear on fracture surfaces (Fig. 5c).

3.3.2. Fatigue fractures

Although SEM studies were inconclusive in discerning any differences in the fatigue and overload fractures, the distinct nature of these two processes was clearly evident in the HVTEM. Examination of failed fatigue specimens and untested control samples revealed a stark difference in the native oxide found at the notch root. In the control samples, a native oxide of ~30 nm in thickness was uniformly distributed over the surfaces of the sample, including the notch. 30-nm thick native oxide layers were also present on the tested fatigue sample, except in the vicinity of the notch where the oxide layer was significantly thicker. Specifically, up to a three-fold increase in oxide thickness at the root of the notch was observed on samples that had been exposed to cyclic stresses (Fig. 6), a result confirmed on three different fatigued samples. Such enhanced notch-root oxidation was not observed in monotonically-loaded samples. Furthermore, no evidence of misfit dislocations due to a compressively-induced phase transformation was observed. As it is conceivable that the high loading frequency and induced electric currents may cause heating in the notch region, the role of thermal effects in the oxidation process was experimentally evaluated (Fig. 7), as discussed below.

By interrupting fatigue specimens prior to failure after testing at various stress amplitudes and examining them with HVTEM, several small cracks (on the order of tens of nanometers in length) were observed within the native oxide at the notch root (Fig. 8). The fact that these cracks were partially through the oxide layer indicates that they are stable cracks; indeed, this is the first evidence of stable fatigue cracking ostensibly in silicon. Moreover, the size of the cracks was consistent with the compliance change of the sample predicted from the finite element modeling

3.3.3. Infrared microscopy

High-resolution (20 mK) infrared images were taken of the test structure during cyclic loading; results at rest and at increasing stress amplitude are shown in Fig. 7. Each image was created by plotting the difference between the IR image at rest and while resonating; the vertical scale represents temperature changes less than 1 K. The slight warming of the mass originates from friction of the silicon with air as the structure resonates at ~40 kHz. However, the temperature of the structure does not rise significantly ($<$1 K) above ambient,

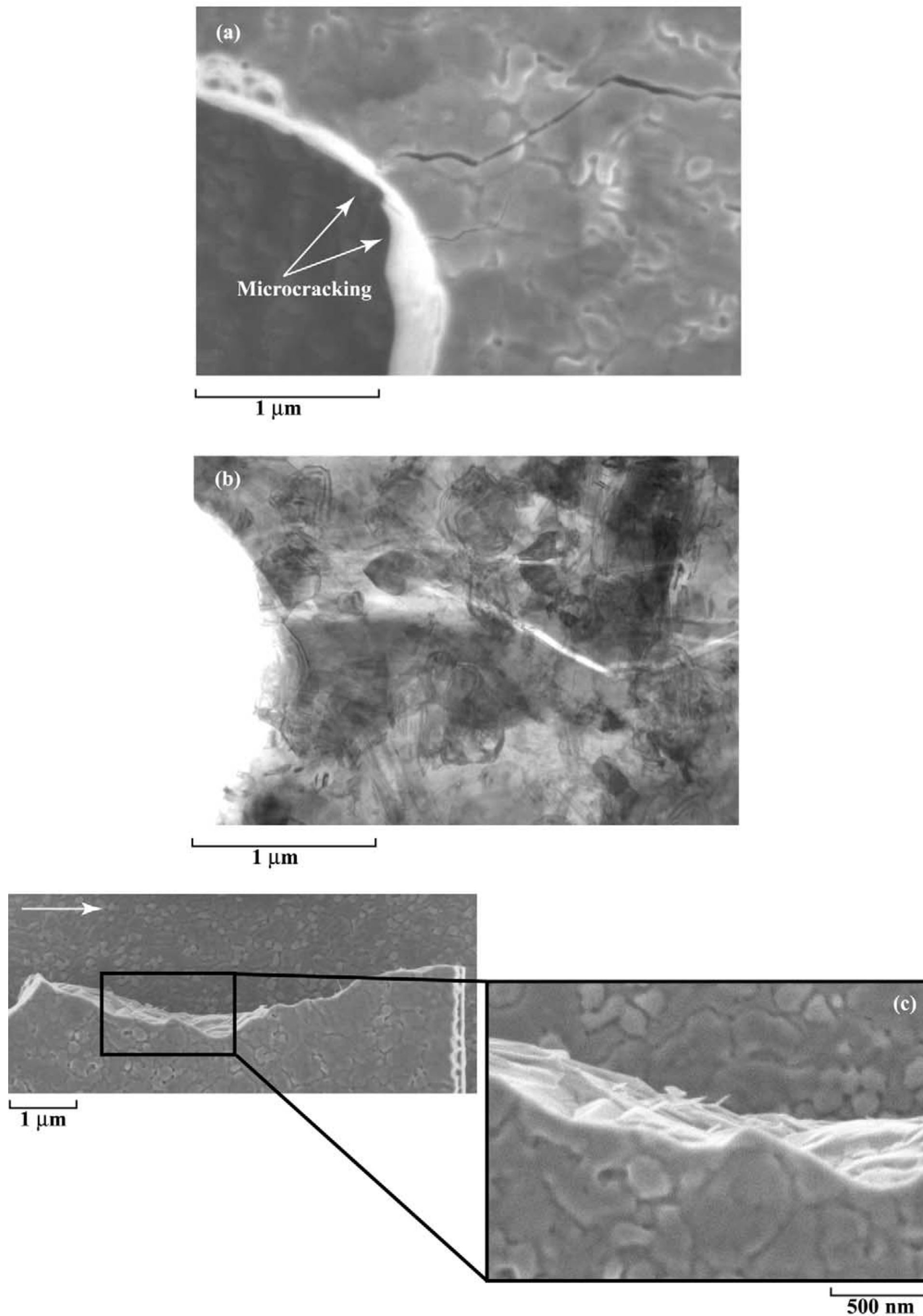

Fig. 5. Fractography of failures in polycrystalline silicon films, showing (a) SEM and (b) HVTEM image of the crack trajectory out of the notch (in an unthinned specimen). (c) SEM images of the transgranular cleavage fracture surfaces of a long-life fatigue test (N_f=3.8×10^{10} cycles at σ_a=2.59 GPa). Horizontal arrow in (c) indicates the direction of crack propagation. Note the fine, needle-like features and debris on the fracture surface in (c).

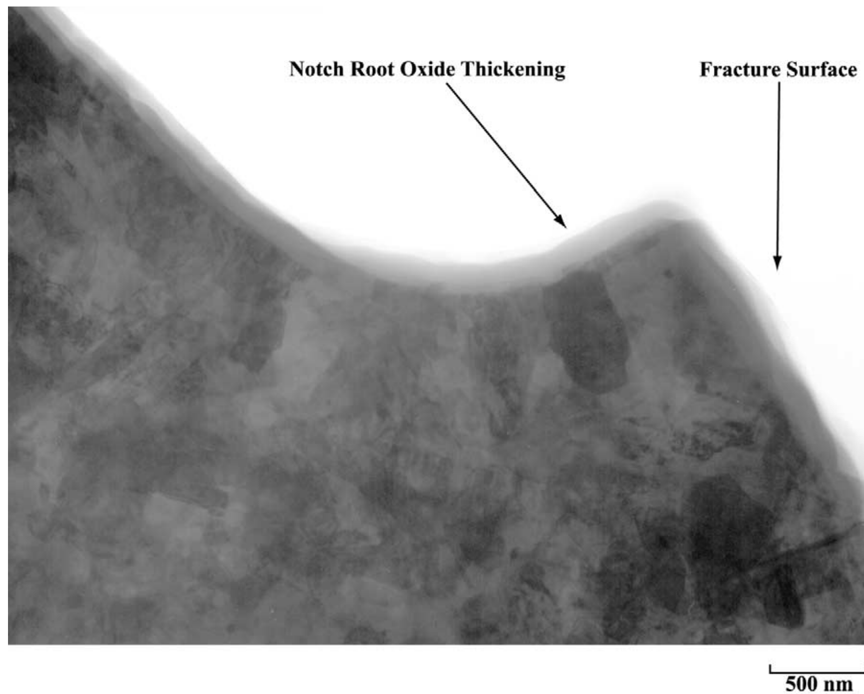

Fig. 6. HVTEM image of the notch region in an unthinned polycrystalline silicon test sample, showing enhanced oxidation at the notch root that failed after 3.56×10^9 cycles at σ_a=2.26 GPa

and there is no measurable change in the notched region. The absence of heating in the cantilever beam section clearly indicates that the enhanced notch-root oxidation is not thermally induced. As the notch root is (initially) the most highly stressed region of the structure, the process appears to be mechanical in origin. Furthermore, since oxide thickening is not observed under quasi-static loading, the phenomenon is associated with the cyclic loading.

3.4. Fracture mechanics analysis

The change in resonant frequency of the cantilever beam was monitored during each test to provide a continuous measure of the specimen compliance. This frequency decreased monotonically (by as much as 50 Hz in the long-life tests) before eventual specimen failure at the notch (Fig. 9). This behavior suggests that the failure of the film occurs after progressive accumulation of damage, e.g., by the stable propagation of a crack. Indeed, the longer the life of the specimen, the larger the decrease in beam stiffness. A method for relating such changes in resonant frequency and damage processes was analyzed in refs. [5] and [25]; in the current work, we utilize this technique to monitor compliance changes quantitatively throughout the fatigue test.

The frequency change, which from experimental observation was reasoned to be due to localized oxidation and cracking at the notch root, was analyzed using plane-stress finite element modal analyses with ANSYS [5]. The model suggested that for ~1 nm of crack extension, a 1 Hz change in natural frequency should be observed. The corresponding model for local notch root oxidation predicted an initial decrease in frequency with increasing oxide layer thickness (at a rate very similar to that induced by cracking) due to the relatively low elastic modulus of the SiO_2; specifically, a 1 nm increase in oxide thickness resulted in a ~0.5 Hz decrease in resonant frequency. The numerical models imply that the measured changes

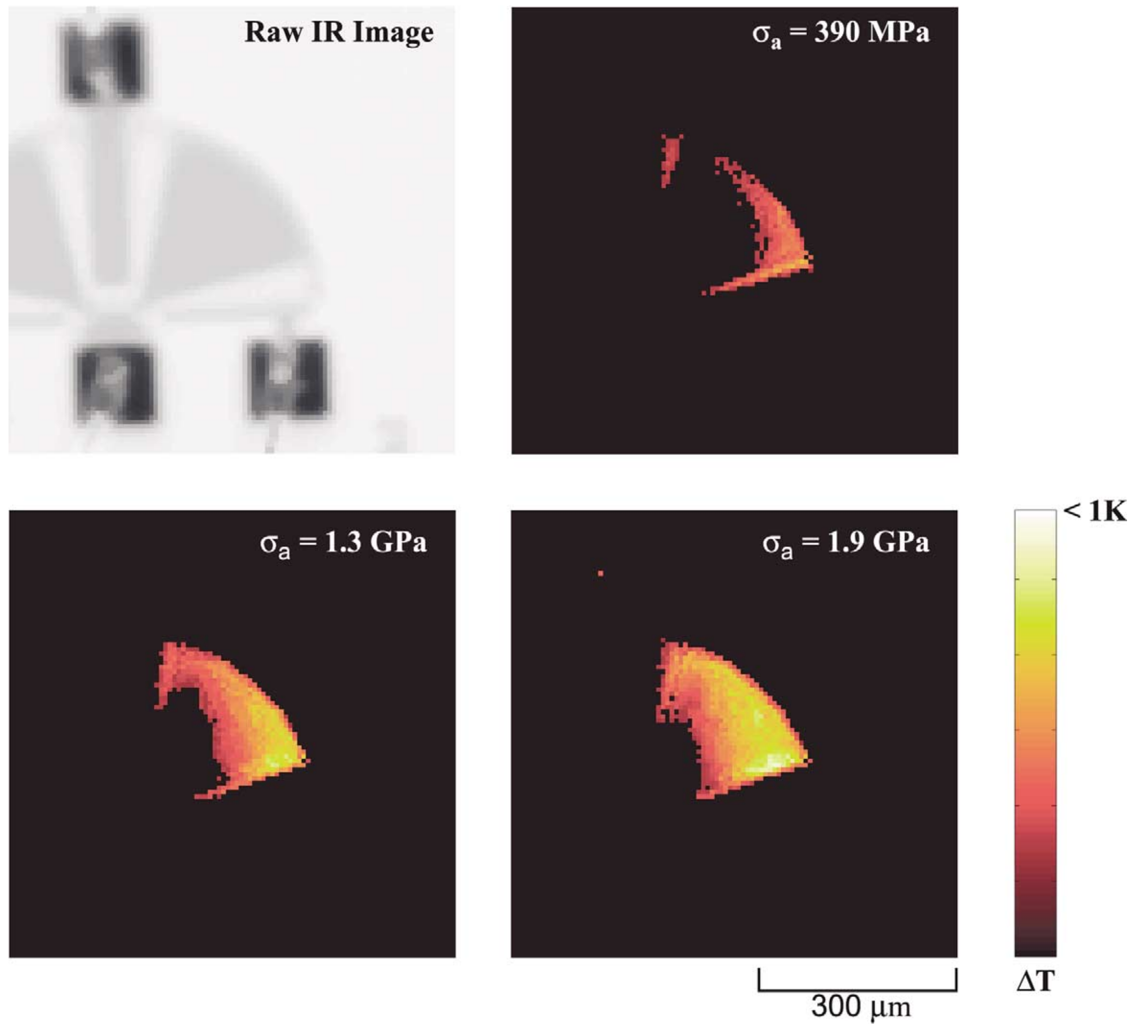

Fig. 7. High resolution (20 mK) infrared (IR) images of the fatigue characterization structure at rest and at increasing stress amplitude at ~40 kHz. Maximum temperature variations were less than 1 K above ambient and were not measurable in the notched cantilever beam specimen.

in resonant frequency are consistent with processes occurring on length scales commensurate with the native oxide thickness. Accordingly, in the present work, estimates of the crack length were made during the tests and are plotted in Fig. 9; these estimates reveal crack sizes that were less than 50 nm throughout the entire fatigue test. As described previously, HVTEM studies provided direct confirmation for these damage processes.

3.4.1. Crack-growth rates

As noted above, in situ measurements of the change in natural frequency during the fatigue test were used to determine the crack length, *a*, as a function of time or cycles [25]. From such data, crack-growth rates, *da/dN*, were calculated over increments of 2 nm in crack extension; a representative result in the form of *da/dN* as a function of *a* is shown in Fig. 10. Crack lengths during the

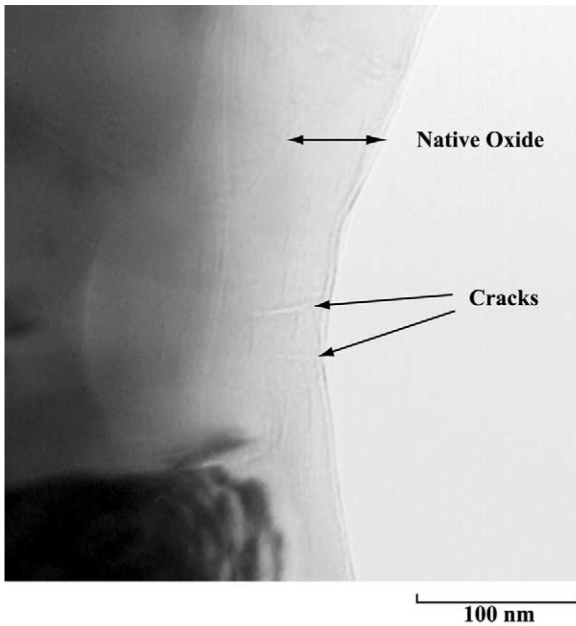

Fig. 8. HVTEM image showing stable cracks, ~50 nm in length, in the native oxide formed during cyclic loading of a notched, polycrystalline silicon beam. Testing of this sample was interrupted after N=3.56×10^9 cycles at a stress amplitude σ_a=2.51 GPa. Image was intentionally defocused to facilitate the observation of the cracks.

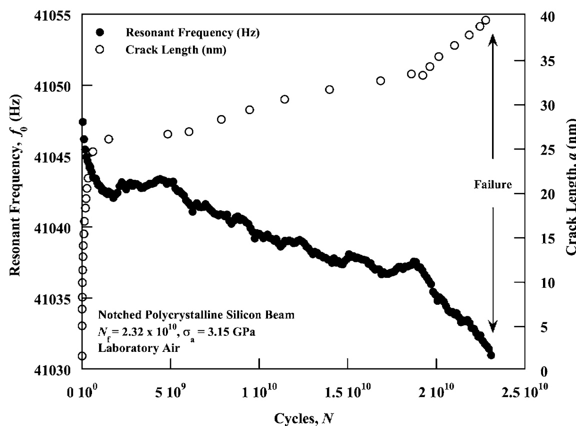

Fig. 9. Representative damage accumulation in polycrystalline silicon, shown by experimentally measured decrease in resonant frequency, f_{crack}, with time during a fatigue test (N_f=2.23×10^{10} cycles at σ_a=3.15 GPa) and the corresponding computed increase in crack length, a.

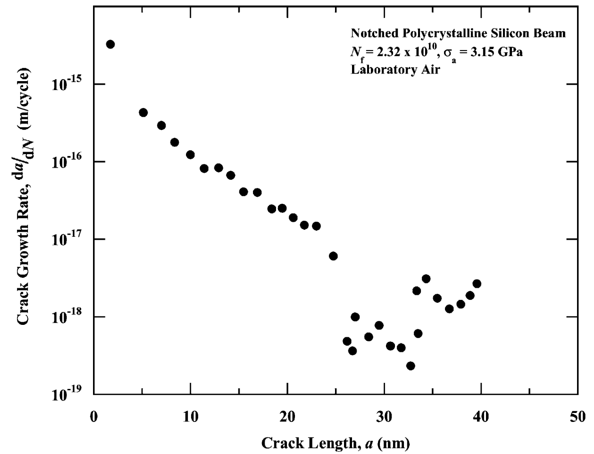

Fig. 10. Representative computed fatigue-crack growth rates, da/dN, as a function of the crack length, a, during a fatigue test of a polycrystalline silicon thin film (N_f=2.32×10^{10} cycles at σ_a=3.15 GPa). Growth rates were determined from the change in specimen compliance monitored throughout the test. Note that the entire fatigue process of crack initiation and growth until the onset of catastrophic failure occurs for crack sizes below ~50 nm, i.e., within the native oxide layer.

fatigue process can be seen to remain under ~50 nm, consistent with the fatigue process occurring in the oxide layer. Growth rates are vanishingly small[1] and progressively decrease with increasing crack length during the test.

3.4.2. Fracture toughness and critical crack size

If the crack-driving force at failure is taken as an estimate of the fracture toughness, the resistance of the material to unstable crack growth can be determined. The crack length estimates at failure were used with plane-strain models of the stress intensity for the notched cantilever beam structure; the relationship between crack length, applied forces, and the stress intensity are detailed in ref. [25]. Results from the polycrystalline silicon

[1] The absolute values of these crack-growth rates are clearly physically unrealistic. However, the growth rates reported are average values associated with the number of cycles at the measured natural frequency (~40 kHz) for the crack to grow over 2 nm increments, assuming that the crack is growing continuously. Although this is the standard way of computing fatigue-crack growth rates [28], in reality the crack may not propagate every cycle and the crack front may not advance uniformly.

fatigue tests (Fig. 11) give an average fracture toughness of ~0.85 MPa√m, consistent with that of the native oxide [29]. However, it is important to note the relationship between the critical crack size at final failure, a_c, and the thickness, h_o, of the SiO_2 reaction layer when K=K_c. Such critical crack sizes are estimated in Fig. 12 for the range of maximum principal stresses used in this investigation. It is apparent that for applied stresses of 2 to 4 GPa, which caused failure in the present films after 10^5 to 10^{11} cycles, the critical crack sizes are less than 50 nm, i.e., comparable to, or less than, the observed oxide layer thicknesses (i.e., $a_c \leq h_o$). *This indicates that the entire process of fatigue-crack initiation, propagation, and the onset of catastrophic (overload) failure all occur within the oxide layer.*

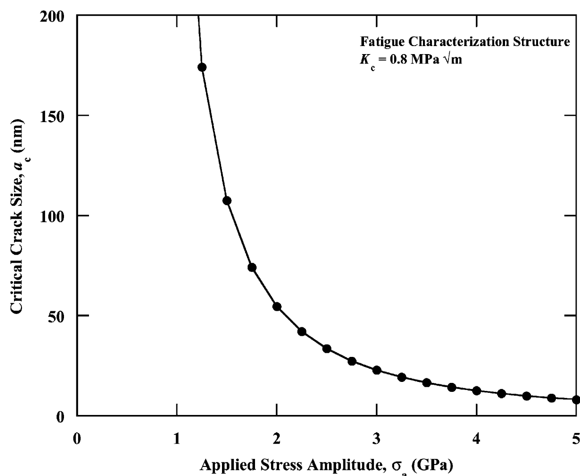

Fig. 12. Computed estimates of the critical crack size, a_c, as a function of the applied stress amplitude, σ_a, in the polycrystalline silicon fatigue characterization structure. Critical crack sizes for the stress amplitudes used in the present tests (σ_a~2 to 4 GPa) are less than ~50 nm, indicating that the onset of final failure of the structure occurs at crack sizes within the native oxide reaction layer.

4. Discussion

4.1. Reaction-layer fatigue

The cyclic fatigue of brittle materials is usually associated with the degradation of (extrinsic) toughening mechanisms in the crack wake [9]. Such toughening arises from crack-tip shielding, which in brittle (non-transforming) ceramic materials generally results from mechanisms such as grain bridging. Under cyclic loading, frictional wear in the sliding grain boundaries can lead to a progressive decay in the bridging stresses (e.g., refs. [9,30,31]). The fatigue of brittle materials is therefore invariably associated with intergranular failure. When such materials fail transgranularly, e.g., as in commercial SiC and sapphire [32,33], there is generally little or no susceptibility to fatigue failure. Since polycrystalline silicon always fails transgranularly [5,21,34], and there has been no reported evidence of extrinsic toughening mechanisms, the material would not be expected to be prone to cyclic fatigue. No precipitates were detected in the silicon films that may also enable conventional, brittle material fatigue mechanisms. Furthermore, below ~500 °C, there is no evidence of mobile dislocation activity [35,36], which could cause fatigue failure as in a ductile material.

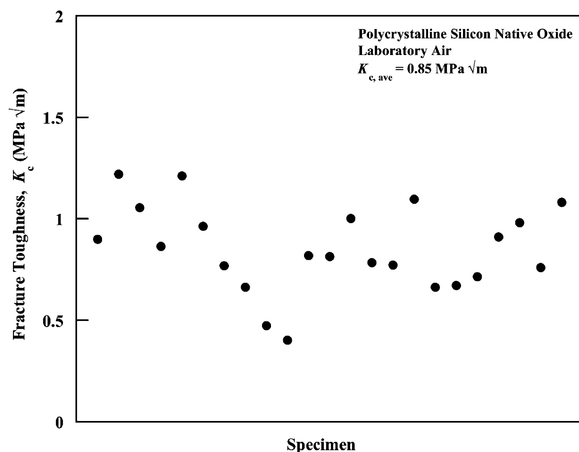

Fig. 11. Computed fracture toughness, K_c, values determined from the estimated crack length immediately prior to failure, i.e., from the critical crack size, a_c, for the given applied stress amplitude. The average fracture toughness of 0.85 MPa√m is consistent with failure within the native oxide on polycrystalline silicon at room temperature.

As the cracks observed in the oxide layer appeared to be quite stable, the cause of this cracking process was reasoned to be environmentally assisted cracking due to the moist air environment. The toughness of the SiO_2 oxide (K_c~0.8 MPa√m)

is comparable to that of the silicon (K_c~1 MPa√m); consequently, it is unlikely that the oxide would crack prematurely and certainly not in the stable manner shown in Fig. 8. However, unlike silicon, amorphous SiO_2 is highly susceptible to environmentally-assisted cracking in moist environments; the threshold stress intensity, K_{scc}, for such cracking is much less than K_c, i.e., typically K_{scc}~0.25 MPa√m, in contrast to silicon where $K_{scc} \approx K_c$ [13–15]. Cyclic effects have also been suggested for subcritical crack growth in borosilicate glass [37]. Since no evidence of dislocation activity near the crack or phase transformations in the vicinity of the notch root were detected, the fatigue of structural silicon films in ambient air is deemed to be associated with stress-corrosion cracking in the native oxide layer that has been thickened under cyclic loading.

We therefore propose that the apparent fatigue of thin-film silicon occurs by a conceptually different mechanism to those cited above for ductile and brittle solids. Specifically, by monitoring the growth of nanoscale cracks with direct HVTEM observation and in situ stiffness changes we conclude that such delayed failures are caused by subcritical cracking of the silica surface layer. The apparent fatigue of thin-film silicon involves the sequential mechanically-induced oxidation and environmentally-assisted cracking of the surface layer, a mechanism that we term *reaction-layer fatigue* (Fig. 13). The native oxide initially forms on the exposed silicon surface with a thickness and composition dictated by the environment and processing history. This native oxide then thickens in high stress regions during subsequent fatigue loading and becomes the site for environmentally assisted cracks which grow stably in the oxide layer. The process then repeats itself until a critical

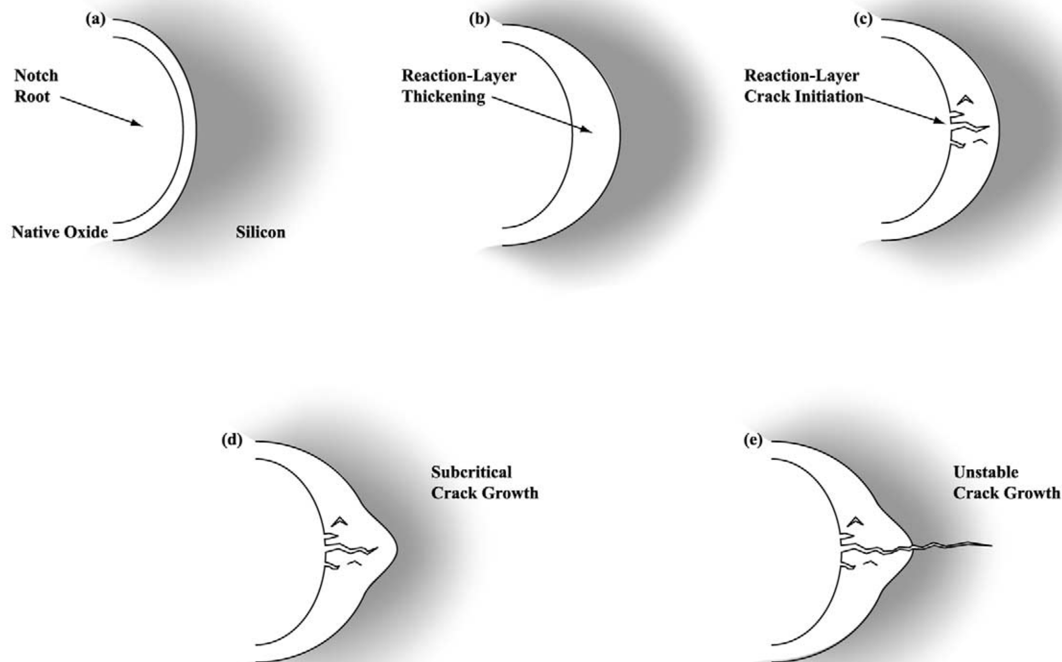

Fig. 13. Schematic illustrations of the reaction-layer fatigue mechanism at the notch of the polycrystalline silicon cantilever beam. (a) Reaction layer (native oxide) on surface of the silicon. (b) Localized oxide thickening at the notch root. (c) environmentally-assisted crack initiation in the native oxide at the notch root. (d) Additional thickening and cracking of reaction layer. (e) Unstable crack growth in the silicon film.

crack size is reached, whereupon the silicon itself fractures catastrophically by transgranular cleavage. The rate-dependence of thin-film silicon fatigue failures is thus dictated by the cycle-dependent oxide thickening process and the time-dependent, environmentally-assisted, subcritical crack growth in this oxide layer.

While thick compared to the native oxide that will typically develop on single crystal silicon at room temperature [38–41], the presence of heavy phosphorous doping and elevated temperature exposure during drying of the film created a significantly thicker reaction layer. However, the precise nature of the mechanically-enhanced oxidation is at present unclear. The notion of a mechanical driving force for oxidation is already a central feature of models for the oxidation of silicon [42–47]. The presence of a compressive stress in the oxide, primarily due to lattice and thermal mismatches, is thought to be responsible for the details of shape effects in oxidation as well as the initially high oxidation rates observed during the early stages of the process [42–47]. However, as most studies have been performed at a high temperature, the role of stress in room temperature oxidation and the importance of cyclic loading are far less clear. Studies of the effect of geometry on oxidation would suggest that the oxide at the notch root should be *thinner* than that found on flat surfaces [46,47]; this further implies the critical role of stress. Furthermore, it is generally accepted that stress can modify the diffusivity of a species in a given material [48]; indeed, high-temperature oxidation studies in silicon suggest contributions on the order of 5–10% of the stress-free activation energy for thermally grown oxides [42–45]. At room temperature, these changes in activation energy would lead to a change in oxidation rate of more than 40 times. As the residual stress distribution in the oxide is dependent on the growth conditions, including the applied stress, it is conceivable that the time-varying stresses encountered during fatigue loading play a role in the oxide thickening. Additionally, the presence of the stress induces cracks within the oxide layer at the notch root which permit the further ingress of moisture and continued oxidation in this region.

The decreasing crack growth-rate behavior observed (Fig. 10) is akin to behavior associated with microstructurally-small cracks, cracks growing under displacement control, cracks growing into residual stress fields, and cracks approaching interfaces. In the present case, the effect is likely related to several of these factors acting *in concert*, as the cracks are certainly small in size, conditions do pertain to displacement control, some degree of residual compression will exist in the SiO_2 layer, and the crack advancing in the oxide is approaching the SiO_2/Si interface where the elastic mismatch between the relatively compliant oxide and the three-fold stiffer silicon substrate will cause the crack to decelerate [49,50].

It is interesting to note that, in principle, the reaction-layer mechanism applies equally to bulk as well as thin-film silicon, even though bulk silicon is generally not considered to be susceptible to either stress-corrosion cracking or fatigue. Cracking in the nano-scale native oxide film has a negligible effect on a macroscopic sample of silicon under load since crack sizes in the oxide could never reach the critical size, i.e., $a_c \gg h_o$, where h_o is the native oxide thickness. In contrast, the surface-to-volume ratio is far larger in micro- and nano-scale samples. Consequently, the oxide layer represents a large proportion of the sample and cracks within the oxide film are readily able to exceed the critical crack size, i.e., $a_c \leq h_o$, as shown quantitatively in Fig. 12. Thus, cracking in the oxide layer alone can lead to failure of the entire silicon component.

This behavior provides insight into the observed *S/N* behavior of thin-film silicon. In metals, the gradual increase in life with decreasing stress amplitude is a direct consequence of the relatively wide range of stable crack growth characterized by a low crack-growth rate exponent of $m \approx 3$–5 in the Paris law, $da/dN = \Delta K^m$ (where ΔK is the stress-intensity range). The appearance of a wide range of lives for bulk brittle materials tested at the same stress amplitude (e.g. [51]) is a natural result of the size distribution of flaws and the limited range for stable fatigue-crack growth in the material, i.e., a large crack-growth rate exponent, $m > 10$ [9]. It is believed that the metal-like *S/N* behavior of silicon is a direct consequence of the decreasing crack-growth rates observed as the crack extends in the

oxide layer. In thin-film silicon the decreasing driving force leads to a range of stable crack growth and failures that change monotonically with decreasing applied stress amplitudes in a measurable timeframe. Although arising from different mechanisms, the correlation between stress amplitude and fatigue life in metals and silicon films is ultimately due to the range of stable crack growth within the timeframe of the tests.

4.2. Suppression of reaction-layer fatigue

The central treatise of this paper is that the fatigue of thin-film silicon is environmentally-induced. Thus, the obvious test of this mechanism is to conduct experiments in an environment where the native oxide cannot form. This poses certain difficulties with the present system, as the removal of the atmosphere affects the damping of the system, causing a mechanical as well as an environmental effect on cracking behavior [25]. An alternative strategy is to use monolayer coatings to suppress the formation of the native oxide with the expectation that such samples would not be susceptible to fatigue in air.

Such coatings have been developed by Maboudian et al. [23,52] to reduce the friction coefficient between contacting silicon surfaces. In the present work, an alkene-based coating of 1-octadecene was used; the 3 nm thick monolayer on the polycrystalline silicon at the root of the notch is shown in Fig. 14. These coatings are applied directly after the silicon is removed from the HF and bond directly with the hydrogen-terminated silicon surface; accordingly, they suppress the formation of the native oxide (Fig. 14). Moreover, they are hydrophobic, stable up to 225 °C, and provide an effective surface barrier to both moisture and oxygen.

The fatigue behavior of thin films of silicon coated with this and other coatings is currently under study. However, initial results on the alkene-based films do show fatigue lifetimes that are essentially unaffected by cyclic stresses (Fig. 4a). Indeed, comparisons of coated and uncoated samples indicate that damage accumulation is dramatically altered and fatigue lives are significantly extended in the coated samples (Fig. 4b). This result clearly provides strong support for the proposed mechanism of silicon fatigue.

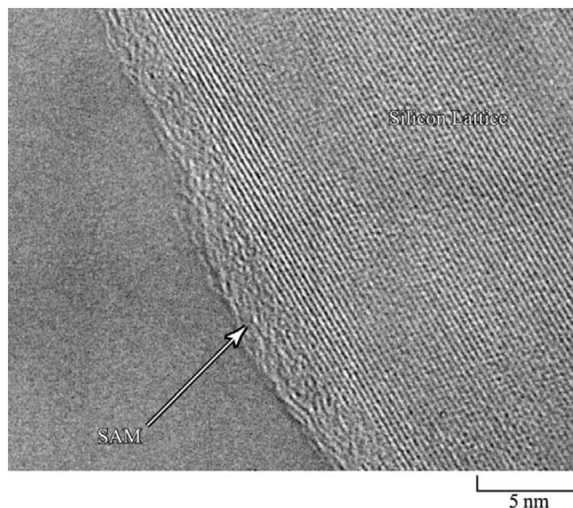

Fig. 14. HVTEM image showing a 1-octadescene self-assembled monolayer (SAM) coating the root of the polycrystalline silicon notch. The lattice fringes of the silicon are clearly visible under the ~3 nm layer that has suppressed the formation of the native oxide layer on the silicon surface.

5. Conclusions

Micron-scale polycrystalline silicon thin films can degrade and prematurely fail by high-cycle fatigue in room air environments. Measured stress/life behavior at ~40 kHz appears to be 'metal-like', with failures occurring at stresses as low as half the (single-cycle) fracture strength for lives in excess of 10^{11} cycles. This presents a significant limitation for the long-term stability and durability of silicon-based MEMS. Based on a study of this high-cycle fatigue phenomenon using 2-μm thick, LPCVD structural films of n^+-type polycrystalline silicon for MEMS applications, the following conclusions can be made:

1. High-voltage transmission electron microscopy (HVTEM) of the polycrystalline silicon thin-film samples revealed a native SiO_2 oxide layer some 30 nm thick. However, during fatigue cycling, this layer was thickened by a factor of roughly three in the immediate vicinity of the

notch root. As high-resolution IR measurements revealed that the temperature of the notch did not exceed 1 K above ambient, such enhanced notch-root oxidation was considered to be primarily mechanically-induced.
2. By stopping fatigue tests for microscopic examination, HVTEM also revealed the presence of stable cracks, tens of nanometers in length, within the enhanced oxide layer. Such subcritical crack growth was reasoned to occur by moisture-induced stress-corrosion cracking in the amorphous SiO_2.
3. In situ monitoring of the change in natural frequency of the fatigue characterization structure during testing was found to be consistent with progressive evolution of damage in the form of oxide formation and subcritical cracking of the oxide. Fracture mechanics-based calibrations using finite element methods revealed crack sizes not exceeding 50 nm, comparable with those imaged directly with HVTEM. This implies that the entire process of fatigue crack initiation, subcritical cracking, and the onset of catastrophic failure, occurs wholly within the native oxide layer.
4. Accordingly, the apparent fatigue of thin-film polycrystalline silicon is ascribed to a 'surface reaction-layer' mechanism involving mechanically-induced oxide thickening and stress-corrosion cracking of the resulting oxide film.
5. Such reaction-layer fatigue is also applicable to bulk silicon although in comparison to thin-film silicon, its effect will be negligible. This is because the high surface-to-volume ratio of the micron-scale films means that the critical crack size for the onset of catastrophic fracture (when $K=K_c$) will occur for cracks within the oxide film. In contrast, the corresponding critical crack size for bulk silicon will be much larger than the native oxide thickness.
6. The susceptibility of thin-film polycrystalline silicon to premature failures under high-cycle fatigue loading can be suppressed through the use of alkene-based monolayer coatings. Such hydrophobic coatings, which bond directly to the hydrogen-terminated silicon surface (created after exposure to HF), inhibit the formation of the oxide layer and further act to prevent the ingress of both moisture and oxygen.

Acknowledgements

This work was funded by the Director, Office of Science, Office of Basic Energy Research, Division of Materials Sciences and Engineering of the US Department of Energy under Contract No. DE-AC03-76SF00098. Additional funding for equipment was provided by Exponent, Inc., Natick, MA, and the New Energy and Industrial Technology Development Organization (NEDO), Tokyo, Japan. The authors wish to thank Dr. S.B. Brown for his initial support, Dr. W. Van Arsdell for the original specimen design, Prof. R. Maboudian and W.R. Ashurst for assistance with the self-assembled monolayer technologies, Drs. M. Enachescu and S. Belikov for help with the IR imaging, and Prof. R.T. Howe and Dr. J.M. McNaney for helpful discussions.

References

[1] Connally JA, Brown SB. Science 1992;256:1537–9.
[2] Brown SB, Van Arsdell W, Muhlstein CL. In: Senturia S, editor. Proceedings of International Solid State Sensors and Actuators Conference (Transducers '97). 1997. p. 591–3.
[3] Muhlstein C, Brown S. Proceedings of the NSF/AFOSR/ASME Workshop on Tribology Issues and Opportunities. In: Bhushan B, editor. MEMS. Kluwer Academic; 1997. p. 80.
[4] Muhlstein, CL, Brown, SB and Ritchie, RO. J. Micrelectromech. Sys., 2001, 10, 593-600.
[5] Muhlstein CL, Brown SB, Ritchie RO. Sens Actuators A 2001;94:177–88.
[6] Kahn H, Ballarini R, Mullen RL, Heuer AH. Proc Roy Soc A 1999;455:3807–23.
[7] Van Arsdell W, Brown SB. J. Micrelectromech. Sys 1999;8:319–27.
[8] Komai K, Minoshima K, Inoue S. Micros. Tech 1998;5:30–7.
[9] Ritchie RO. Int. J. Fract 1999;100:55–83.
[10] Suresh, S., Fatigue of Materials. 2nd ed., Cambridge University Press, Cambridge, England, 1998.
[11] Ritchie RO, Dauskardt RH. J. Ceram. Soc. Jap 1991;99:1047–62.
[12] Kahn H, Tayebi N, Ballarini R, Mullen RL, Heuer AH. Sens. Actuators A 2000;A82:274–80.

[13] Chen TJ, Knapp WJ. J. Am. Ceram. Soc 1980;63:225–6.
[14] Lawn BR, Marshall DB, Chantikul P. J. Mater. Sci 1981;16:1769–75.
[15] Wong B, Holbrook RJ. J. Electrochem. Soc 1987;134:2254–6.
[16] Allameh SM, Gally B, Brown S, Soboyejo WO. In: Kahn H, de Boer M, Judy M, Spearing SM, editors. Materials Science of Microelectromechanical System (MEMS) Devices III. MRS; 2000. p. EE2.
[17] Kato NI, Nishikawa A, Saka H. Advanced characterisation of semiconductor materials. Elsevier, 2000 pp. 113-115.
[18] Muhlstein CL, Stach EA, Ritchie RO, Appl Phys Let, 2002, 80, 1532–1534.
[19] MCNC/Cronos, www.memsrus.com, 2000.
[20] Simmons G, Wang H. Single crystal elastic constants and calculated aggregate properties: a handbook, 2nd ed. Cambridge, MA: M.I.T. Press, 1971.
[21] Ballarini R, Mullen RL, Yin Y, Kahn H, Stemmer S, Heuer AH. Adv. Appl. Mech 1997;12:915–22.
[22] Bravman JC, Sinclair R. J. Electron. Micr. Tech 1984;1:53.
[23] Ashurst WR, Yau C, Carraro C, Maboudian R, Dugger MT. J. Micrelectromech. Sys 2001;10:41–9.
[24] Van Arsdell W. Ph.D. dissertation, Massachusetts Institute of Technology, 1997.
[25] Muhlstein CL, Howe RT, Ritchie RO. Mech. Mater., 2002, in review.
[26] Sharpe Jr. WN, Yuan B, Edwards RL. In: Suhling JC, Liechti KM, Liu S, editors. Proceedings of 1997 International Mechanical Engineering Congress and Exposition. ASME; 1997. p. 113–6.
[27] Mikkelsen JC. In: Mikkelsen JC, Pearton SJ, Corbett JW, Pennycook SJ, editors. Oxygen, Carbon, Hydrogen and Nitrogen in Crystalline Silicon. MRS; 1986. p. 3–5.
[28] ASTM. E 647 standard test method for measurement of fatigue crack growth rates. In: Annual Book of ASTM Standards, 03.01. West Conshohocken, PA: ASTM; 2001.
[29] Wiederhorn SM. In: Valluri SR, Taplin DMR, Ramo Rao R, Knott JF, Dubey R, editors. Advances in Fracture Research. Pergamon Press; 1984. p. 61-3.
[30] Dauskardt RH. Acta Metal Mater 1993;41:2765–81.
[31] Lathabai S, Rödel J, Lawn BR. J Am Ceram Soc 1991;74:1340–8.
[32] Gilbert CJ, Cao JJ, MoberlyChan WJ, DeJonghe LC, Ritchie RO. Acta Mater 1996;44:3199–214.
[33] Asoo B, McNaney JM, Mitamura Y, Ritchie RO. J. Biomed. Mater. Res., 2000, 488-491.
[34] Chen CP, Leipold MH. Amer. Cer. Soc. Bull 1980;59:469–72.
[35] Lawn BR, Hockey BJ, Wiederhorn SM. J. Mater. Sci. Sci 1980;15:12.
[36] Chiao YH, Clarke DR. Acta Metal 1989;37:203–19.
[37] Dill SJ, Bennison SJ, Dauskardt RH. J. Am. Ceram. Soc. 1997;80:773–6.
[38] Taft EA. J. Electrochem. Soc 1988;135:1022–3.
[39] Lukes F. Surf. Sci 1972;30:91–100.
[40] Raider SI, Flitsch R, Palmer MJ. J. Electrochem. Soc 1975;122:413–8.
[41] Lu ZH, Sacher E, Yelon A. Phil. Mag. B 1988;58:385–8.
[42] Fargeix A, Ghibaudo G. J. Appl. Phys 1983;54:7153–8.
[43] Fargeix A, Ghibaudo G, Kamarinos G. J. Appl. Phys 1983;54:2878–80.
[44] Fargeix A, Ghibaudo G. J. Phys. D 1984;17:2331–6.
[45] Fargeix A, Ghibaudo G. J. Appl. Phys 1984;56:589–91.
[46] Kao D, McVittie JP, Nix WD, Saraswat KC. IEEE Trans. Elect. Dev. 1987;ED-34:1008–17.
[47] Kao DB, McVittie JP, Nix WD, Saraswat KC. IEEE Trans. Elect. Dev. 1988;ED-35:25–37.
[48] Paul W, Warschauer DM. Solids under pressure. New York, NY: McGraw-Hill, 1963.
[49] Hutchinson JW, Suo Z. Adv. Appl. Mech 1992;29:63–163.
[50] Beuth Jr. JL. Int J Solids Struct 1992;29:1657–75.
[51] Lathabai S, Yiu-Wing M, Lawn BR. J. Am. Ceram. Soc 1989;72:1760–3.
[52] Ashurst WR, Yau C, Carraro C, Howe RT, Maboudian R. Hilton Head Solid-State Sensor and Actuator Workshop. Transducers Res. Found, 2000 pp. 320-323.